J Braz. Soc. Mech. Sci. Eng. (2017) 39:737–756
DOI 10.1007/s40430-016-0554-2

TECHNICAL PAPER

Numerical JModelica.org-based approach to a simulation of Coriolis effects on guided boom-driven payload swaying during non-uniform rotary crane boom slewing

Alexander A. Kostikov[1] · Alexander V. Perig[2] · Denys Yu. Mikhieienko[3] · Ruslan R. Lozun[2,3]

Received: 27 January 2016 / Accepted: 26 April 2016 / Published online: 3 June 2016

Abstract The present article is focused on the study of the swaying motion of a payload during non-uniform guided slewing of a crane boom with an emphasis on the Coriolis effects. A new mathematical model of the motion of the mechanical system "guided crane boom–payload" has been derived with an introduction of Blajer's projection method. The governing dynamic system has been shown in the form of an implicit system of differential-algebraic equations. A time-optimal control problem has been formulated for the guided system with an open-loop control and with explicit limitations on payload swaying and on the control input. The numerical solution of the posed optimization problem has been found with an introduction of Optimica and JModelica.org freeware. Verification of numerically derived results has been realized through the comparison of computational and experimental absolute trajectories of a swaying payload. A satisfactory agreement between theoretical and experimental results was found. A dynamic analogy between the governing system of equations and Foucault pendulum-like systems was found and outlined. The proposed open code algorithms, derived numerical data and computational plots enhance and expand our knowledge about the dynamics of guided boom-driven payload swaying during rotary crane boom slewing.

Keywords Payload swaying · Crane boom slewing · Open-loop optimal control problem · JModelica.org · Optimica · Freeware

List of symbols

DAE	Differential algebraic equation
point A_{st}	Point of static equilibrium of payload M at the cable BM
point M	Point of position of payload M in the current moment of time
point D	Initial point of crane boom BD and center of circle for trajectory of transport and absolute motion for the point B
point B	Terminal point of crane boom BD
m	Mass of payload M (kg)
g	Scalar value of gravitational acceleration (m/s^2)
$u(t)$	Control input voltage at the windings of the rotary AC-servo motor (V)
u_{max}	Maximum value of control input voltage (V)
t	Current swaying time for payload M (s)
T	Period of slewing for crane boom BD (s)
t_f	The final time of rotation of crane boom BD with attached to p. B payload M at final angular displacement φ_e (s)

Technical Editor: Kátia Lucchesi Cavalca Dedini.

✉ Alexander V. Perig
olexander.perig@gmail.com;
alexander.perig@dgma.donetsk.ua

[1] Informatics and Engineering Graphics Department, Donbass State Engineering Academy, Shkadinova 72, Kramatorsk, Donetsk Region 84313, Ukraine

[2] Manufacturing Processes and Automation Engineering Department, Donbass State Engineering Academy, Shkadinova 72, Kramatorsk, Donetsk Region 84313, Ukraine

[3] Computer and Information Technology Department, Donbass State Engineering Academy, Shkadinova 72, Kramatorsk, Donetsk Region 84313, Ukraine

T_φ	Time constant of rotary AC-servo motor, where the numerical value of time constant $T_\varphi = 0.015$ (s) is provided in Table 2, page 1181 of Ref. [10] by Terashima et al. (2007) (s)
K_φ	Gain of rotary AC-servo motor, where the numerical value of gain $K_\varphi = 0.315$ [1/(sV)] is provided in Table 2, page 1181 of Ref. [10] by Terashima et al. (2007) [1/(sV)]
J	Minimized functional for final time of crane boom rotation (s)
$J = t_\mathrm{f}$	Notation for time-optimal control problem (s)
$(x_1(t), \ldots, x_8(t))$	The phase variables of dynamic system, where dimensions of the phase variables are determined by formulae (14)–(21) and are as follows: ($x_1(t)$, $x_3(t)$ and $x_5(t)$) are in (m); $x_7(t)$ is in (rad); ($x_2(t)$, $x_4(t)$ and $x_6(t)$) are in (m/s); $x_8(t)$ is in (rad/s)
ε	The maximum value of payload swaying during crane boom BD slewing at the certain final angular displacement $(\varphi_\mathrm{e})_\mathrm{f}$, which is determined by the restrictive inequality $(x_1(t))^2 + (x_3(t))^2 + (x_5(t))^2 \le \varepsilon$ on the phase variables ($x_1(t)$, $x_3(t)$, $x_5(t)$) (m^2)
$\mathscr{E}$	Motionless fixed on earth inertial reference frame $O_2x_2^*y_2^*z_2^*$ $(O_2x_\mathrm{abs}y_\mathrm{abs}z_\mathrm{abs})$ with origin in p. O_2 and the orthogonal unit vectors $\hat{\mathrm{e}}_1$; $\hat{\mathrm{e}}_2$; $\hat{\mathrm{e}}_3$, where $x_2^* = x_\mathrm{abs}$; $y_2^* = y_\mathrm{abs}$ $z_2^* = z_\mathrm{abs}$ are the absolute coordinates of payload M with respect to Earth (m)
$\mathscr{B}$	Non-inertial reference frame $(O_1x_1y_1z_1)$, which is connected with rotating crane boom BD with origin in p. O_1 (p. A_st) and the orthogonal unit vectors $\tilde{\mathbf{e}}_1$; $\tilde{\mathbf{e}}_2$; $\tilde{\mathbf{e}}_3$, where x_1; y_1; z_1 are the relative coordinates of payload M with respect to crane boom BD (m)
$R = \mathrm{BD}$	Boom length in the horizontal plane ($\hat{\mathbf{e}}_1$, $\hat{\mathbf{e}}_2$) (m)
$l = l_\mathrm{BM} = \lVert\mathbf{r}_\mathrm{B/M}\rVert$	Length of the cable BM, i.e., the magnitude of the position vector $\mathbf{r}_\mathrm{B/M}$ (m)
r_comp	The magnitude of the radius-vector, connecting point O_2 and theoretical ($J = t_\mathrm{f}$)-based computational absolute trajectory of payload M in Figs. 6 and 7
$r_\mathrm{exper} = r_\mathrm{emp}$	The magnitude of the radius-vector, connecting point O_2 and experimentally (or empirically) derived absolute trajectory of payload M in Figs. 6 and 7
r_circle	The radius of standard circular trajectory of p. B (p. $\mathrm{A_{st}}$) in Figs. 6 and 7
$\varphi_\mathrm{e} = \angle(\hat{\mathbf{e}}_1, \tilde{\mathbf{e}}_2)$	Angle of rotation of non-inertial reference frame $\mathscr{B}$ around axis $O_2z_2^*$ (O_2z_abs) of inertial reference frame $\mathscr{E}$, i.e., the angle of transport rotation for crane boom BD around the vertical axis $O_2z_2^*$ (O_2z_abs), i.e., crane boom slewing angle (rad)
$\alpha_1 = \angle(\tilde{\mathbf{e}}_3, \mathbf{r}_\mathrm{B/M})$	Swaying angle between the vertical axis O_1z_1 and the position vector $\mathbf{r}_\mathrm{B/M}$, i.e., the first spherical coordinate of spherical pendulum M (rad)
α_2	Swaying angle between the planes (x_1z_1) and (BMO_1), i.e., the second spherical coordinate of spherical pendulum M (rad)
$(\alpha_1, \alpha_2, \varphi_\mathrm{e})$	The angular coordinates of spherical pendulum M with rotating pivot center in p. B connect to crane boom tip (rad)
$\boldsymbol{\omega}_{\mathscr{B}/\mathscr{E}}$	Angular velocity vector of reference frame $\mathscr{B}$ with respect to frame $\mathscr{E}$, i.e., the vector of slewing velocity of crane boom BD (rad/s)
$\omega_{\mathscr{B}/\mathscr{E}} = \omega_\mathrm{e} = \mathrm{d}\varphi_\mathrm{e}/\mathrm{d}t$	Scalar of transport angular velocity of reference frame $\mathscr{B}$ with respect to frame $\mathscr{E}$, i.e., the value of slewing velocity of crane boom BD (rad/s)
ω_max	Maximum value of angular velocity of reference frame $\mathscr{B}$ with respect to frame $\mathscr{E}$, i.e., the maximum value of slewing velocity of crane boom BD (rad/s)
$\boldsymbol{\omega}_{\mathscr{B}/\mathscr{E}} = \boldsymbol{\omega}_\mathbf{e} = (\mathrm{d}\varphi_\mathrm{e}/\mathrm{d}t)\hat{\mathbf{e}}_3$	Transport slewing angular velocity vector of reference frame $\mathscr{B}$ with respect to frame $\mathscr{E}$, i.e., the vector of slewing velocity of crane boom BD (rad/s)

$\boldsymbol{\varepsilon}_{\mathscr{B}/\mathscr{E}} = \boldsymbol{\alpha}_{\mathscr{B}/\mathscr{E}}$	Angular acceleration vector of reference frame $\mathscr{B}$ with respect to frame $\mathscr{E}$, i.e., the vector of slewing acceleration of crane boom BD (rad/s^2)
$\alpha_{\mathscr{B}/\mathscr{E}} = \varepsilon_e = \mathrm{d}^2\varphi_e/\mathrm{d}t^2$	Scalar of transport angular acceleration of reference frame $\mathscr{B}$ with respect to frame $\mathscr{E}$, i.e., the value of slewing acceleration of crane boom BD (rad/s^2)
$\boldsymbol{\varepsilon}_{\mathscr{B}/\mathscr{E}} = \boldsymbol{\varepsilon}_{\mathbf{e}} = (\mathrm{d}^2\varphi_e/\mathrm{d}t^2)\mathbf{e_3}$	Transport angular acceleration vector of reference frame $\mathscr{B}$ with respect to frame $\mathscr{E}$, i.e., the vector of slewing acceleration of crane boom BD (rad/s^2)
$\mathbf{V}_{M/\mathscr{E}} = \mathbf{V}_{\mathbf{abs}}$	Velocity of point M in inertial fixed on earth reference frame $\mathscr{E}$, i.e., absolute velocity of payload M (m/s)
$\mathbf{V}_{M/\mathscr{B}} = \mathbf{V}_{\mathbf{r}}$	Velocity of point M in non-inertial reference frame $\mathscr{B}$, i.e., relative velocity of payload M (m/s)
$\mathbf{V}_{\mathbf{e}} = \mathbf{V}_{O_2/\mathscr{E}} + \omega_{\mathscr{B}/\mathscr{E}} \times \mathbf{r}_{O_2/M}$	Transport velocity of point M in inertial reference frame $\mathscr{E}$, i.e., the linear velocity of the "frozen" point M, which being "frozen" to crane boom BD "lost its relative velocity" and moves together with slewing non-inertial reference frame $\mathscr{B}$ with respect to inertial reference frame $\mathscr{E}$ (m/s)
V_{x_1}; V_{y_1}; V_{z_1}	X_1-, y_1-, z_1- projections of payload M velocity in non-inertial reference frame $\mathscr{B}$ (m/s)
$\mathbf{a}_{M/\mathscr{E}} = \mathbf{a}_{\mathbf{abs}}$	Acceleration of point M in inertial fixed on earth reference frame $\mathscr{E}$, i.e., absolute acceleration of payload M (m/s^2)
$\mathbf{a}_{M/\mathscr{B}} = \mathbf{a}_{\mathbf{r}}$	Acceleration of point M in non-inertial reference frame $\mathscr{B}$, i.e., relative acceleration of payload M (m/s^2)
$\mathbf{a}_{\mathbf{e}}^{\tau} = \boldsymbol{\alpha}_{\mathscr{B}/\mathscr{E}} \times \mathbf{r}_{o_2/M}$	Tangential acceleration of transportation for payload M (m/s^2)
$\mathbf{a}_{\mathbf{e}}^{\mathbf{n}} = \boldsymbol{\omega}_{\mathscr{B}/\mathscr{E}} \times \left(\boldsymbol{\omega}_{\mathscr{B}/\mathscr{E}} \times \mathbf{r}_{o_2/M}\right)$	Normal or centripetal acceleration of transportation for payload M (m/s^2)
$\mathbf{a}_{\mathrm{cor}} = 2\boldsymbol{\omega}_{\mathscr{B}/\mathscr{E}} \times \mathbf{V}_{M/\mathscr{B}}$	Coriolis (compound) acceleration of payload M (m/s^2)
$\mathbf{mg}$	Gravitational force (N)
$\mathbf{N}$	Reaction force of the cable BM (N)
$\boldsymbol{\Phi}_{\mathbf{e}}^{\tau} = (-\mathrm{m})\mathbf{a}_{\mathbf{e}}^{\tau}$	Tangential inertial force (tangential force of moving space) for payload M (N)
$\boldsymbol{\Phi}_{\mathbf{e}}^{\mathbf{n}} = (-\mathrm{m})\mathbf{a}_{\mathbf{e}}^{\mathbf{n}}$	Normal or centrifugal inertial force (normal force of moving space) for payload M [N]
$\boldsymbol{\Phi}_{\mathbf{cor}} = (-\mathrm{m})\mathbf{a}_{\mathbf{cor}}$	Coriolis inertial force (compound centrifugal force) for payload M (N)
δ	Relative dimensionless amplitude discrepancy between computational and experimental absolute trajectories of point M in the inertial reference frame $\mathscr{E}$
$\delta_{\max}$	The maximum value of δ
JModelica (JModelica.org)	Computational freeware code for time-optimal control problem solution, available at http://www.jmodelica.org/
Optimica	The integrated part of JModelica (JModelica.org) freeware

1 Introduction

1.1 The state of the art and review

The dynamic problem of guided payload swaying during controlled slewing of a crane boom is the main priority inverse problem of crane dynamics for allowable motion and accurate positioning of loaded boom cranes [1–10]. This problem is closely associated with the primary problem of inverse dynamics of a pendulum with a rotating pivot center, where a law of guided rotational motion of the pendulum pivot center is unknown a priori and depends on the control input variable $u(t)$. A review of relevant published works has identified a number of research efforts, which have been focused on various aspects of allowable payload swaying during guided crane boom slewing [1–10].

The direct solution approach is used by Benson et al. for the reduction of the optimal control problem to a nonlinear programming problem through the introduction of the Gauss pseudospectral method [1]. Use of this method results in the possibility to achieve rapid convergence with a small increase in sampling points required for quantization and enables easy accounting of limitations on the control and phase variables [1].

Blajer et al. have addressed the problem of payload motion control as it applies to payload path definition [2]. The control problem in Blajer's approach is posed in the following way. The control variables which ensure the transportation of a payload along the prescribed trajectory are determined without minimization of payload motion time and without taking into account the Coriolis effects. Blajer et al. get the different control parameters in

dependence of prescribed trajectory [2]. The principal fundamental difference between our problem and Blajer's is that we don't know the trajectory of payload motion and we have to minimize the time of payload transportation from the initial to final position. Moreover, the Blajer's solution does not ensure minimization of payload transportation time during payload transportation from the initial to final position [2].

Condurache et al. have proposed an exact vector solution of the driven Foucault pendulum problem and derived a new conservation law for Foucault pendulum-like motions through an introduction of differential and vector computations [3]. This study made a complex comprehensive investigation of Foucault pendulum motion in a central force field with respect to a non-inertial reference frame fixed on earth [3].

JModelica.org is an open source freeware platform for optimization, simulation and analysis of complex dynamic systems [4]. JModelica.org is based on the Modelica simulation language [4]. The key feature of JModelica.org is Optimica extension [4]. Optimica provides the user the capability for the easy formulation of optimization problems by grounding the problems for optimization on Modelica's model for natural determination of the optimization interval, the goal function and constraints [4]. A very essential benefit from the Optimica extension is Optimica's possibility for working with differential equations, which describe the behavior of dynamic systems and are written in the unresolved form for the first derivative [4]. This useful possibility broadens the class of problems which could be solved with the JModelica.org platform [4].

Palis and Palis have studied open-loop and closed-loop control strategies for crane boom slewing motion [5]. Both linear and nonlinear models for slewing cranes and swaying payload motions with open-loop control were studied [5]. Coriolis and centrifugal effects have been taken into account in this study for a nonlinear model of a crane boom–payload system with open-loop control [5]. A time-optimal control problem was posed and solved by the authors with a linear model of the crane boom–payload system with open-loop control [5]. They then found the absolute trajectory of the payload motion for a nonlinear model through the use of a linear model-derived solution of a time-optimal control problem for an open-loop system [5]. So a linear model-derived optimal control solution was applied to the nonlinear case for an open-loop system and an essential discrepancy was found between the linear and nonlinear models in the final point of payload displacement [5]. As result, taking into account these discrepancies between linear and nonlinear models, the authors proposed a damping strategy for the system with closed-loop control, which made it possible to reduce payload oscillations after the crane boom stops [5]. However, they did not solve the time-optimal control problem for the nonlinear model of a crane boom–payload system taking Coriolis and centrifugal effects for open-loop control into account. So the work [5] by Palis and Palis did not allow minimization of payload swaying during crane boom slewing.

Perig et al. derived and confirmed the relative and absolute trajectories for payload swaying, taking into account the effect of Coriolis inertia forces [6, 7]. However, Perig's approach was mainly focused on the cases of uniform crane boom slewing and did not properly address the crane boom control problem [6, 7].

Pontryagin (also written Pontriagin or Pontrjagin) et al. have formulated Pontryagin's (Pontriagin's or Pontrjagin's) maximum principle, which represents a necessary condition for optimal control problems [8]. This principle is based on establishing a connection between objective-optimized functional and process dynamics [8]. This connection is realized through the use of the Hamiltonian function [8]. According to Pontryagin's (Pontriagin's or Pontrjagin's) maximum principle for optimal control and for corresponding coordinates for which the optimum criterion has a minimum, the Hamiltonian function has a maximum [8]. Pontryagin's (Pontriagin's or Pontrjagin's) maximum principle is widely used for the solution of optimal control problems but there are difficulties with its usage when limitations exist on the phase variables, in addition to the control variables. The direct solution method is another computational technique, which is also used for the solution of optimal control problems [1]. The direct solution method is reduced to switching the optimal control problem to a nonlinear programming problem [1].

Sakawa et al. have proposed a model for payload swaying during crane boom slewing with the introduction of open-loop control [9]. Sakawa et al. have proposed a new numerical solution of the optimal control problem for payload swaying during crane boom slewing through the introduction of an additional penalty function and cost functional [9]. However, Sakawa's computational approach has some special features [9]. Sakawa's work [9] is focused on the determination of optimal control for minimization of payload swaying both during crane boom slewing, and at the end of crane boom angular displacement. Sakawa et al. have proposed the following computational technique in the search for the optimal control. Sakawa et al. have converted the optimal control problem to a boundary value problem for a system of differential equations through an introduction of the Pontryagin (Pontriagin or Pontrjagin) maximum principle [8] with further application of different algorithms for initial conditions assignment. The high accuracy of the solution and the guarantee that the solution satisfies optimality conditions of the first order are the advantages of this method [9]. However, this technique has a number of shortcomings, namely, the small radius of

convergence. So there is a need to choose the first initial approximation to be near the optimum. Moreover, difficulties with this approach have arisen when taking into account the constraints on the phase and control variables. Sakawa et al. have applied the hyperplane constraint technique in order to take into account the available constraints on the phase variables. In this way Sakawa et al. have converted two constraints on the phase variables to constraints on the phase and control variables. This causes distortion of the region of permissible values for phase and control variables. Moreover, the algorithm of control time minimization in Sakawa's work is different from the algorithm of optimal control search with fixed time. This fact rather complicates the usage of Sakawa's algorithm in other applications. Moreover, Sakawa addressed the method of penalty functions in order to take into account the one remaining constraint. And this Sakawa's approach complicates the form of the minimized functional. However, the proposed computational technique is a quite abstract and complex one. Sakawa's approach has no adaptation to engineering practice due to the absence of simple engineering formulae for payload swaying values. Moreover, the absolute swaying trajectories have not been derived for crane boom slewing angles [0° … 180°] in Fig. 3 at p. 552, in Fig. 5 at p. 554, in Fig. 7 at p. 555, and in Fig. 8 at p. 555 of Sakawa's work [9].

Terashima et al. determined the necessary control for crane boom rotation, crane boom lifting, and cable length change for payload displacement from initial to final positions with minimum time [10]. However, Terashima's dynamic model for payload motion does not properly account for the influence of the Coriolis inertia force on payload swaying [10].

1.2 Aims and scopes of the present research

The above-mentioned literature review has shown that the nonlinear problem of payload swaying during guided crane boom slewing, taking nonlinear Coriolis effects into account, has not been properly addressed in previous known research [1–10]. This fact emphasizes the prime novelty and actuality of the present article, which is focused on formulation and proposing a freeware-based numerical solution of open-loop time-optimal control nonlinear problem with accent on Coriolis force-influence effects on relative and absolute payload motion.

The main goal of the present article is focused on the formulation, posing and freeware-based numerical solution of an open-loop time-optimal control nonlinear problem of payload swaying during crane boom-guided slewing with proper accounting of nonlinear Coriolis effects.

The object of this research is the process of payload swaying along the Coriolis force-influenced trajectory during crane boom-guided slewing for an open-loop crane boom drive system.

The subject of research is focused on the general trends of open-loop time-optimal control derived relative and absolute trajectories of swaying payload with respect to non-uniform unknown law of crane boom slewing, and nonlinear Coriolis effects during payload swaying motion.

1.3 Prime novelty statement of research (highlights)

The main contribution of this article to the field is as follows.

The present article is focused on the mathematical formulation and the derivation of a numerical solution of the DAE-based open-loop optimal control problem for payload-guided swaying during crane boom non-uniform slewing.

The prime novelty of this article is as follows.

For the first time a numerical solution of the open-loop optimal control problem for boom-driven payload transportation during crane boom slewing from the initial to the final position with minimum transportation time has been derived with an application of Optimica and JModelica.org open source freeware, where a dynamic model of the guided payload swaying takes into account the effects of Coriolis force influence on the relative and absolute trajectories of the guided swaying payload. The influence of the allowable payload swaying ε on the control parameter of the crane boom drive has been clarified. The present article extends the ideas about adaptability of Foucault pendulum-like systems for the problems of open-loop optimal control for swaying of the spherical pendulum with rotating pivot center. The complex of authors-proposed computational algorithms was implemented with free scientific software Optimica and JModelica.org. The proposed open code algorithms derived numerical data and computational plots for open-loop optimal control problem enhance and expand our knowledge about the dynamics of guided boom-driven payload swaying during rotary crane boom slewing.

The present paper has the possible industrial applications in R&D-related fields of transport engineering and carrying-and-lifting machinery.

2 Computational approach

2.1 Mechanical formulation of the problem and the governing equations

We will study a 3D model of the boom crane shown in Fig. 1. This model is a 3DOF mechanical system, which

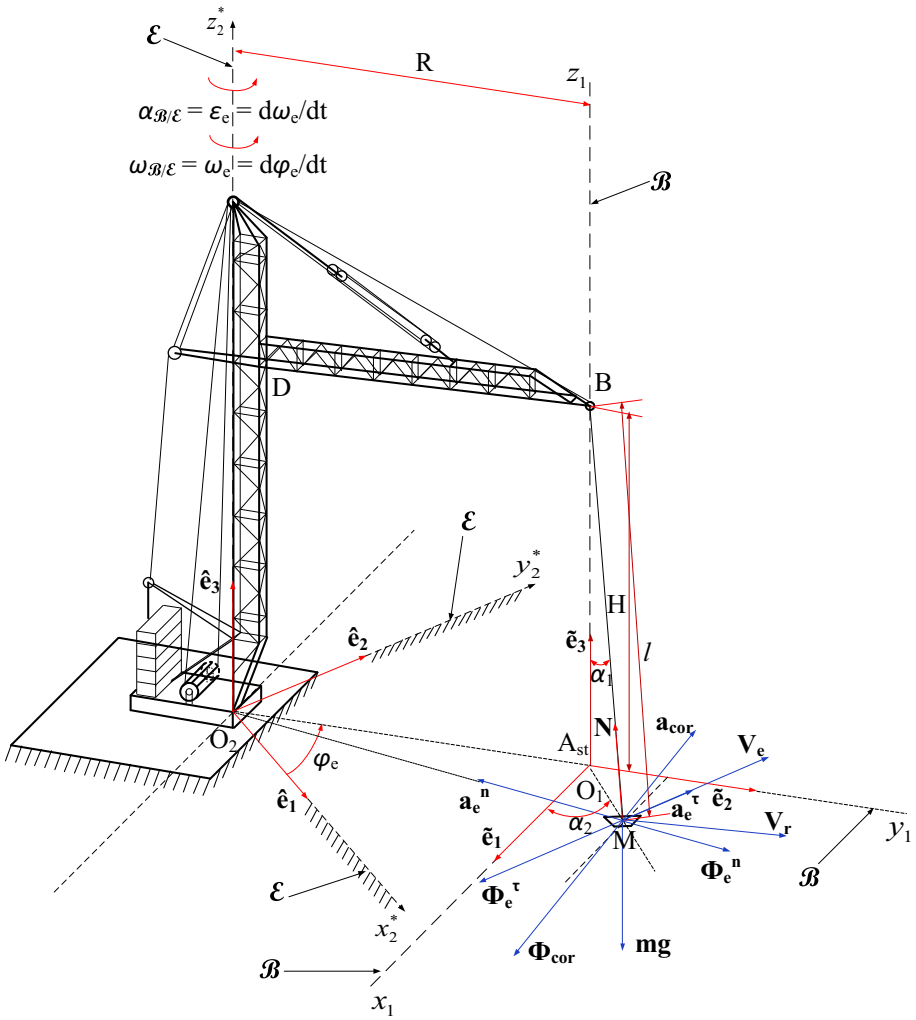

Fig. 1 The computational scheme of payload M swaying during guided crane boom DB slewing accounting for nonlinear effects, caused by inertia forces $\mathbf{\Phi}_e^\tau$, $\mathbf{\Phi}_e^n$ and $\mathbf{\Phi}_{cor}$

includes slewing boom BD, cable BM, connected to the boom tip B, and swaying payload M, suspended to cable BM (Fig. 1). The motion of a dynamic mechanical system "crane boom–payload" is described in Fig. 1. This system has the following three degrees of freedom: crane boom BD slewing angle $\varphi_e(t)$ [rad], and relative angular coordinates $\alpha_1(t)$ [rad] and $\alpha_2(t)$ [rad] for swaying payload M, where the one control input parameter $u(t)$ [V] is the rotary AC-servo motor winding voltage and the one control input $u(t)$ determines the first $(d(\varphi_e(t))/dt)$ [rad/s] and the second $(d^2(\varphi_e(t))/dt^2)$ [rad/s^2] derivatives of crane boom BD slewing angle $\varphi_e(t)$ [rad], as well as the angle $\varphi_e = \varphi_e(t)$ of crane boom slewing (detailed description of $\varphi_e(t)$, $(d(\varphi_e(t))/dt)$, $(d^2(\varphi_e(t))/dt^2)$, $\alpha_1(t)$ and $\alpha_2(t)$ is shown in the Nomenclature chapter). It is possible to describe the position of payload M, attached to the boom crane BD with four dependent coordinates

$$\mathbf{p}(t) = [\varphi_e(t),\ x_1(t),\ y_1(t),\ z_1(t)]^{\circ T}, \tag{1}$$

where $\mathbf{p}(t)$ is the positional vector of payload M, $\varphi_e(t)$ is the crane boom BD slewing angle and $(x_1(t), y_1(t), z_1(t))$ are Cartesian relative coordinates of payload M in the non-inertial reference frame $\mathcal{B}$, connected with the crane boom BD tip B (Fig. 1).

The coordinate $\varphi_e(t)$ also determines crane boom BD position without payload M as if payload M is non-existent. There is the following geometric constraint, imposed on the relative coordinates $(x_1(t), y_1(t), z_1(t))$ of payload M and the transport coordinate $\varphi_e(t)$ of crane boom BD:

$$\Phi(x_1(t),\ y_1(t),\ z_1(t), t) = \sqrt{(x_1(t))^2 + (y_1(t))^2 + (z_1(t) - l)^2} - l = 0. \tag{2}$$

We will derive the dynamic equations of motion of mechanical system "crane boom BD–payload M" using the projection method, proposed by Blajer et al. [2]. We will write equations of unconstrained motion of crane boom BD and payload M without taking into account the geometric constraint (2). The first equation of the governing system is Terashima's [10] equation, which establishes the relationship between crane boom BD angular

acceleration $(d^2(\varphi_e(t))/dt^2)$, crane boom BD angular velocity $(d(\varphi_e(t))/dt)$ and control input voltage $u(t)$:

$$\left(\frac{d^2(\varphi_e(t))}{dt^2}\right) = -\left(\frac{1}{T_\varphi}\right)\left(\frac{d(\varphi_e(t))}{dt}\right) + \left(\frac{K_\varphi}{T_\varphi}\right)(u(t)), \quad (3)$$

where Eq. (3) and numerical values of $T_\varphi = 0.015$ [s] and $K_\varphi = 0.315$ [1/(sV)] in Eq. (3) are written on the basis of Terashima's Eqs. (1)–(2) and Terashima's Table 2 at page 1181 of Ref. [10] by Terashima et al., and $u(t)$ is the control input voltage at the windings of the rotary AC-servo motor.

The second equation of the governing system is the dynamic equation of relative unconstrained motion of payload M with respect to the non-inertial reference frame $\mathscr{B}$. This equation does not coincide with the dynamic Coriolis theorem in the absence of reaction of constraint (2) in it, i.e., as if constraint (2) is not imposed on payload M at all:

$$m\mathbf{a}_r = m\mathbf{g} + \left(-m\mathbf{a}_e^\tau\right) + \left(-m\mathbf{a}_e^n\right) + \left(-m\mathbf{a}_{cor}\right), \quad (4)$$

where $\mathbf{g}$ is the vector of gravitational acceleration, $\mathbf{a}_r = \mathbf{a}_{M/\mathscr{B}}$ is the vector of relative acceleration of payload M in the non-inertial reference frame $\mathscr{B}$, $\mathbf{a}_e^\tau = \boldsymbol{\alpha}_{\mathscr{B}/\mathscr{E}} \times \mathbf{r}_{o_2/M}$ and $\mathbf{a}_e^n = \boldsymbol{\omega}_{\mathscr{B}/\mathscr{E}} \times \left(\boldsymbol{\omega}_{\mathscr{B}/\mathscr{E}} \times \mathbf{r}_{o_2/M}\right)$ are tangential and normal accelerations for the motion of the non-inertial reference frame $\mathscr{B}$ with respect to the motionless fixed on earth inertial reference frame $\mathscr{E}$, and $\mathbf{a}_{cor} = 2\boldsymbol{\omega}_{\mathscr{B}/\mathscr{E}} \times \mathbf{V}_{M/\mathscr{B}}$ is the Coriolis acceleration of payload M, caused by the slewing motion of the non-inertial reference boom-connected frame $\mathscr{B}$ with respect to the inertial reference frame $\mathscr{E}$, where

$$\mathbf{a}_r = \mathbf{a}_{M/\mathscr{B}} = \left(\frac{d^2(x_1(t))}{dt^2}\right)\tilde{\mathbf{e}}_1 + \left(\frac{d^2(y_1(t))}{dt^2}\right)\tilde{\mathbf{e}}_2 + \left(\frac{d^2(z_1(t))}{dt^2}\right)\tilde{\mathbf{e}}_3; \quad (5)$$

$$\mathbf{a}_e^\tau = \boldsymbol{\alpha}_{\mathscr{B}/\mathscr{E}} \times \mathbf{r}_{O_2/M} = \left(-\left(\frac{d^2(\varphi_e(t))}{dt^2}\right)(R + y_1(t))\right)\tilde{\mathbf{e}}_1 + \left(\left(\frac{d^2(\varphi_e(t))}{dt^2}\right)x_1(t)\right)\tilde{\mathbf{e}}_2; \quad (6)$$

$$\mathbf{a}_e^n = \boldsymbol{\omega}_{\mathscr{B}/\mathscr{E}} \times (\boldsymbol{\omega}_{\mathscr{B}/\mathscr{E}} \times \mathbf{r}_{O_2/M}) = \left(-\left(\frac{d(\varphi_e(t))}{dt}\right)^2 x_1(t)\right)\tilde{\mathbf{e}}_1 - \left(\left(\frac{d(\varphi_e(t))}{dt}\right)^2 (R + y_1(t))\right)\tilde{\mathbf{e}}_2; \quad (7)$$

$$\mathbf{a}_{cor} = 2\boldsymbol{\omega}_{\mathscr{B}/\mathscr{E}} \times \mathbf{V}_{M/\mathscr{B}} = \left(-2\left(\frac{d(\varphi_e(t))}{dt}\right)\left(\frac{d(y_1(t))}{dt}\right)\right)\tilde{\mathbf{e}}_1 + \left(2\left(\frac{d(\varphi_e(t))}{dt}\right)\left(\frac{d(x_1(t))}{dt}\right)\right)\tilde{\mathbf{e}}_2. \quad (8)$$

The distinctive key feature of the present work is accounting for the Coriolis inertia force $\boldsymbol{\Phi}_{cor} = (-m)\mathbf{a}_{cor}$ [N] and the assumption about fixed cable BM length $l = \text{const}$ [m] during crane boom BD transport slewing motion with an arbitrary angular velocity $\boldsymbol{\omega}_{\mathscr{B}/\mathscr{E}} = \boldsymbol{\omega}_e \neq \mathbf{const}$ [rad/s] and with simultaneous relative swaying of payload M in Fig. 1 [detailed description of inertia forces $\boldsymbol{\Phi}_e^\tau = (-m)\mathbf{a}_e^\tau$ [N], $\boldsymbol{\Phi}_e^n = (-m)\mathbf{a}_e^n$ [N] and $\boldsymbol{\Phi}_{cor} = (-m)\mathbf{a}_{cor}$ [N] is shown in the Nomenclature chapter and in the above listed formulae (6)–(8)].

It is possible to project a vector Eq. (4) for unconstrained motion of payload M to the coordinate axes (x_1, y_1, z_1) of the non-inertial reference frame $\mathscr{B}$ by taking into account vector Eqs. (5)–(8) for accelerations:

$$m\left(\frac{d^2(x_1(t))}{dt^2}\right) = m\left(\left(\frac{d^2(\varphi_e(t))}{dt^2}\right)(R + y_1(t))\right) + m\left(\left(\frac{d(\varphi_e(t))}{dt}\right)^2 x_1(t)\right) + 2m\left(\left(\frac{d(\varphi_e(t))}{dt}\right)\left(\frac{d(y_1(t))}{dt}\right)\right); \quad (9)$$

$$m\left(\frac{d^2(y_1(t))}{dt^2}\right) = -m\left(\left(\frac{d^2(\varphi_e(t))}{dt^2}\right)x_1(t)\right) + m\left(\left(\frac{d(\varphi_e(t))}{dt}\right)^2 (R + y_1(t))\right) - 2m\left(\left(\frac{d(\varphi_e(t))}{dt}\right)\left(\frac{d(x_1(t))}{dt}\right)\right); \quad (10)$$

$$m\left(\frac{d^2(z_1(t))}{dt^2}\right) = -mg. \quad (11)$$

According to Blajer's approach [2], it is possible to write the system of ordinary differential Eqs. (3), (9)–(11) for unconstrained crane boom BD and unconstrained payload M in the following matrix form:

$$\mathbf{M}\left(\frac{d^2(\mathbf{p}(t))}{dt^2}\right) = \mathbf{f}(t) - \mathbf{B}^T u(t), \quad (12)$$

where $\mathbf{M}$ is the diagonal 4×4 generalized mass matrix, $(d^2(\mathbf{p}(t))/dt^2)$ is the 4-component vector of acceleration of payload M, $\mathbf{f}(t)$ is the 4-component vector of generalized applied active and inertia forces, $\mathbf{B}^T$ is the 4-component control vector, and $u(t)$ is the control input voltage, where

$$\mathbf{M} = \begin{bmatrix} 1 & 0 & 0 & 0 \\ 0 & m & 0 & 0 \\ 0 & 0 & m & 0 \\ 0 & 0 & 0 & m \end{bmatrix}; \quad (13)$$

$$\left(\frac{\mathrm{d}^2(\mathbf{p}(t))}{\mathrm{d}t^2}\right)=\left[\left(\frac{\mathrm{d}^2(\varphi_{\mathrm{e}}(t))}{\mathrm{d}t^2}\right),\ \left(\frac{\mathrm{d}^2(x_1(t))}{\mathrm{d}t^2}\right),\ \left(\frac{\mathrm{d}^2(y_1(t))}{\mathrm{d}t^2}\right),\ \left(\frac{\mathrm{d}^2(z_1(t))}{\mathrm{d}t^2}\right)\right]^{\mathrm{T}};\tag{14}$$

$$\mathbf{f}(t)=\begin{pmatrix}-\left(\frac{1}{T_\varphi}\right)\left(\frac{\mathrm{d}(\varphi_{\mathrm{e}}(t))}{\mathrm{d}t}\right)\\ m\left(\left(\frac{\mathrm{d}^2(\varphi_{\mathrm{e}}(t))}{\mathrm{d}t^2}\right)(R+y_1(t))\right)+m\left(\left(\frac{\mathrm{d}(\varphi_{\mathrm{e}}(t))}{\mathrm{d}t}\right)^2x_1(t)\right)+2m\left(\left(\frac{\mathrm{d}(\varphi_{\mathrm{e}}(t))}{\mathrm{d}t}\right)\left(\frac{\mathrm{d}(y_1(t))}{\mathrm{d}t}\right)\right)\\ -m\left(\left(\frac{\mathrm{d}^2(\varphi_{\mathrm{e}}(t))}{\mathrm{d}t^2}\right)x_1(t)\right)+m\left(\left(\frac{\mathrm{d}(\varphi_{\mathrm{e}}(t))}{\mathrm{d}t}\right)^2(R+y_1(t))\right)-2m\left(\left(\frac{\mathrm{d}(\varphi_{\mathrm{e}}(t))}{\mathrm{d}t}\right)\left(\frac{\mathrm{d}(x_1(t))}{\mathrm{d}t}\right)\right)\\ -mg\end{pmatrix};\tag{15}$$

$$\mathbf{B}^{\mathrm{T}}=\left[\left(-\left(\frac{K_\varphi}{T_\varphi}\right)\right),\ 0,\ 0,\ 0\right]^{\mathrm{T}}.\tag{16}$$

However, the real mechanical system "crane boom BD–payload M" contains the imposed geometric constraint (2) in the shape of the cable BM. So the real problem of payload M swaying during crane boom BD slewing requires us to take into account the presence of an imposed geometric constraint (2) by imposition of geometric constraint (2) at divided subsystems "crane boom BD" and "payload M". In this case Blajer's dynamic Eq. (12) for an unconstrained system should be written in modified form to take into account the presence of reaction $\lambda(t)$ of cable BM constraint. Blajer et al. have proposed the following modified dynamic equation:

$$\mathbf{M}\left(\frac{\mathrm{d}^2(\mathbf{p}(t))}{\mathrm{d}t^2}\right)=\mathbf{f}(t)-\mathbf{B}^{\mathrm{T}}u(t)-\left(\mathbf{C}^{\mathrm{T}}(\mathbf{p})\right)\lambda(t),\tag{17}$$

where $\mathbf{C}^{\mathrm{T}}(\mathbf{p})=\partial\Phi/\partial\mathbf{p}$ is the 4-component constraint vector, and $\lambda(t)$ is the undetermined Lagrange multiplier, where

$$\mathbf{C}^{\mathrm{T}}(\mathbf{p})=\left[0,\ \left(\frac{x_1(t)}{l}\right),\ \left(\frac{y_1(t)}{l}\right),\ \left(\frac{z_1(t)-l}{l}\right)\right]^{\mathrm{T}}.\tag{18}$$

The scalar form of Blajer's matrix Eq. (17) for the motion of constrained system "crane boom BD–payload M" can be formulated by taking into account the above written formulae (3), (9)–(18) and in our case is as follows:

$$\left(\frac{\mathrm{d}^2(\varphi_e(t))}{\mathrm{d}t^2}\right)=-\left(\frac{1}{T_\varphi}\right)\left(\frac{\mathrm{d}(\varphi_{\mathrm{e}}(t))}{\mathrm{d}t}\right)+\left(\frac{K_\varphi}{T_\varphi}\right)(u(t)),\tag{19}$$

$$\begin{aligned}m\left(\frac{\mathrm{d}^2(x_1(t))}{\mathrm{d}t^2}\right)&=m\left(\left(\frac{\mathrm{d}^2(\varphi_{\mathrm{e}}(t))}{\mathrm{d}t^2}\right)(R+y_1(t))\right)\\&+m\left(\left(\frac{\mathrm{d}(\varphi_{\mathrm{e}}(t))}{\mathrm{d}t}\right)^2x_1(t)\right)\\&+2m\left(\left(\frac{\mathrm{d}(\varphi_{\mathrm{e}}(t))}{\mathrm{d}t}\right)\left(\frac{\mathrm{d}(y_1(t))}{\mathrm{d}t}\right)\right)\\&-(\lambda(t))\left(\frac{x_1(t)}{l}\right);\end{aligned}\tag{20}$$

$$\begin{aligned}m\left(\frac{\mathrm{d}^2(y_1(t))}{\mathrm{d}t^2}\right)&=-m\left(\left(\frac{\mathrm{d}^2(\varphi_{\mathrm{e}}(t))}{\mathrm{d}t^2}\right)x_1(t)\right)\\&+m\left(\left(\frac{\mathrm{d}(\varphi_{\mathrm{e}}(t))}{\mathrm{d}t}\right)^2(R+y_1(t))\right)\\&-2m\left(\left(\frac{\mathrm{d}(\varphi_{\mathrm{e}}(t))}{\mathrm{d}t}\right)\left(\frac{\mathrm{d}(x_1(t))}{\mathrm{d}t}\right)\right)\\&-(\lambda(t))\left(\frac{y_1(t)}{l}\right);\end{aligned}\tag{21}$$

$$m\left(\frac{\mathrm{d}^2(z_1(t))}{\mathrm{d}t^2}\right)=-mg-(\lambda(t))\left(\frac{z_1(t)-l}{l}\right),\tag{22}$$

where $\lambda(t)=N(t)$ is the reaction of the constraint BM, i.e., the cable BM tension force.

It is possible to eliminate $\lambda(t)$ from (17), (19)–(22) through the use of Blajer's projection method. For this purpose we will project the Blajer's dynamic Eq. (17) in the instantaneous direction, perpendicular to the surface of the constraint (2). The perpendicular direction to the surface of the constraint (2) is determined by the vector $\mathbf{C}^{\mathrm{T}}(\mathbf{p})$ (18). Following Blajer's approach we will compute the scalar product of Eq. (17) at the vector $\mathbf{C}(\mathbf{p})$ (18). As result we will get the following dynamic expression:

$$\begin{aligned}\left((\mathbf{C}(\mathbf{p})),\mathbf{M}\left(\frac{\mathrm{d}^2(\mathbf{p}(t))}{\mathrm{d}t^2}\right)\right)&=((\mathbf{C}(\mathbf{p})),\mathbf{f}(t))\\&-\left((\mathbf{C}(\mathbf{p})),\mathbf{B}^{\mathrm{T}}u(t)\right)\\&-\left((\mathbf{C}(\mathbf{p})),\left(\mathbf{C}^{\mathrm{T}}(\mathbf{p})\right)\lambda(t)\right),\end{aligned}\tag{23}$$

where $(\mathbf{C}(\mathbf{p}),\ \mathbf{C}^{\mathrm{T}}(\mathbf{p}))=1$.

So dynamic expression (23) yields the following formula for cable tension $\lambda(t)=N(t)$:

$$\begin{aligned}\lambda(t)=&((\mathbf{C}(\mathbf{p})),\mathbf{f}(t))-\left((\mathbf{C}(\mathbf{p})),\mathbf{B}^{\mathrm{T}}u(t)\right)\\&-\left((\mathbf{C}(\mathbf{p})),\mathbf{M}\left(\frac{\mathrm{d}^2(\mathbf{p}(t))}{\mathrm{d}t^2}\right)\right).\end{aligned}\tag{24}$$

The coordinate form of the Eq. (24) in our case is as follows:

$$\lambda(t) = \left(\frac{x_1(t)}{l}\right)\left[m\left(\left(\frac{\mathrm{d}^2(\varphi_e(t))}{\mathrm{d}t^2}\right)(R + y_1(t))\right) + m\left(\left(\frac{\mathrm{d}(\varphi_e(t))}{\mathrm{d}t}\right)^2 x_1(t)\right) + 2m\left(\left(\frac{\mathrm{d}(\varphi_e(t))}{\mathrm{d}t}\right)\left(\frac{\mathrm{d}(y_1(t))}{\mathrm{d}t}\right)\right) - m\left(\frac{\mathrm{d}^2(x_1(t))}{\mathrm{d}t^2}\right)\right] + \left(\frac{y_1(t)}{l}\right)\left[-m\left(\left(\frac{\mathrm{d}(\varphi_e(t))}{\mathrm{d}t^2}\right)x_1(t)\right) + m\left(\left(\frac{\mathrm{d}(\varphi_e(t))}{\mathrm{d}t}\right)^2 (R + y_1(t))\right) - 2m\left(\left(\frac{\mathrm{d}(\varphi_e(t))}{\mathrm{d}t}\right)\left(\frac{\mathrm{d}(x_1(t))}{\mathrm{d}t}\right)\right) - m\left(\frac{\mathrm{d}^2(y_1(t))}{\mathrm{d}t^2}\right)\right] - \left(\frac{z_1(t) - l}{l}\right)\left[mg + m\left(\frac{\mathrm{d}^2(z_1(t))}{\mathrm{d}t^2}\right)\right]. \quad (25)$$

After substitution of derived expression (25) for cable tension force $\lambda(t) = N(t)$ into dynamic Eqs. (20)–(22), we will get a new system of equations, which does not depend on $\lambda(t)$. So it is possible to formulate the time-optimal control problem for dynamic system of Eqs. (19)–(22), (25) with eliminated cable tension force $\lambda(t) = N(t)$.

The present control problem is focused on the nonlinear character of the mechanical problem in Fig. 1, where system nonlinearities are determined by the nonlinear nature of cable tension force $\mathbf{N}(t)$ and the nonlinear effect of Coriolis inertia force $\mathbf{\Phi}_{\mathbf{cor}}$.

2.2 Mathematical formulation of the time-optimal control problem

We will determine the phase variables in the following way:

$$x_1(t) = x_1(t); \quad (26)$$

$$x_2(t) = \frac{\mathrm{d}(x_1(t))}{\mathrm{d}t}; \quad (27)$$

$$x_3(t) = y_1(t); \quad (28)$$

$$x_4(t) = \frac{\mathrm{d}(y_1(t))}{\mathrm{d}t}; \quad (29)$$

$$x_5(t) = z_1(t); \quad (30)$$

$$x_6(t) = \frac{\mathrm{d}(z_1(t))}{\mathrm{d}t}; \quad (31)$$

$$x_7(t) = \varphi_e(t); \quad (32)$$

$$x_8(t) = \frac{\mathrm{d}(\varphi_e(t))}{\mathrm{d}t}. \quad (33)$$

Using this notation, we formulate the optimal control problem.

It is necessary to find the optimal control input $u(t)$ that gives the minimum for the function

$$J = t_f; \quad (34)$$

and takes the state from the initial position to the final one for the system, subjected to the following constraints:

$$\frac{\mathrm{d}(x_1(t))}{\mathrm{d}t} = x_2(t); \quad (35)$$

$$\frac{\mathrm{d}(x_2(t))}{\mathrm{d}t} = x_8^2(t) \cdot x_1(t) + (K_1 \cdot x_8(t) + K_2 \cdot u(t)) \cdot (R + x_3(t)) + 2 \cdot x_8(t) \cdot x_4(t) - \left(\frac{N(t)}{m}\right) \cdot \left(\frac{x_1(t)}{l}\right); \quad (36)$$

$$\frac{\mathrm{d}(x_3(t))}{\mathrm{d}t} = x_4(t); \quad (37)$$

$$\frac{\mathrm{d}(x_4(t))}{\mathrm{d}t} = x_8^2(t) \cdot (R + x_3(t)) - (K_1 \cdot x_8(t) + K_2 \cdot u(t)) \cdot x_1(t) - 2 \cdot x_8(t) \cdot x_2(t) - \left(\frac{N(t)}{m}\right) \cdot \left(\frac{x_3(t)}{l}\right); \quad (38)$$

$$\frac{\mathrm{d}(x_5(t))}{\mathrm{d}t} = x_6(t); \quad (39)$$

$$\frac{\mathrm{d}(x_6(t))}{\mathrm{d}t} = -g + \left(\frac{N(t)}{m}\right) \cdot \left(\frac{(l - x_5(t))}{l}\right); \quad (40)$$

$$\frac{\mathrm{d}(x_7(t))}{\mathrm{d}t} = x_8(t); \quad (41)$$

$$\frac{\mathrm{d}(x_8(t))}{\mathrm{d}t} = K_1 \cdot x_8(t) + K_2 \cdot u(t); \quad (42)$$

$$(x_1(t))^2 + (x_3(t))^2 + (x_5(t))^2 \le \varepsilon; \quad (43)$$

$$x_1(0) = 0; \quad x_2(0) = 0; \quad x_3(0) = 0; \quad x_4(0) = 0; \quad x_5(0) = 0; \quad x_6(0) = 0; \quad x_7(0) = 0; \quad x_8(0) = 0; \quad (44)$$

$$x_1(t_f) = 0; \quad x_2(t_f) = 0; \quad x_3(t_f) = 0; \quad x_4(t_f) = 0; \quad x_5(t_f) = 0; \quad x_6(t_f) = 0; \quad x_7(t_f) = \pi; \quad x_8(t_f) = 0; \quad (45)$$

$$|u(t)| \le u_{\max}; \quad |x_8(t)| \le \omega_{\max}; \quad (46)$$

where

$$K_1 = \frac{1}{t_f}; \quad (47)$$

$$K_2 = \frac{K_f}{t_f}; \tag{48}$$

Terashima et al. addressed the "clipping-off" gradient algorithm in order to take into account the limitations on the control variables [10].

$$N(t) = ml\left[\left(\frac{\left(x_1(t)\cdot\left(\frac{\mathrm{d}x_2(t)}{\mathrm{d}t}\right)+x_2^2(t)+x_3(t)\cdot\left(\frac{\mathrm{d}x_4(t)}{\mathrm{d}t}\right)+x_3^2(t)\right)}{\left(l^2-x_1^2(t)-x_3^2(t)\right)}\right)+\left(\frac{\left(x_1(t)\cdot x_2(t)+x_3(t)\cdot x_4(t)\right)^2}{\left(l^2-x_1^2(t)-x_3^2(t)\right)^2}\right)\right] + \frac{mgl}{\sqrt{\left(l^2-x_1^2(t)-x_3^2(t)\right)}} \tag{49}$$

The initial position is determined by (44), the final position is determined by (45), Eqs. (35)–(42) of this system (35)–(46) have been derived from (19) to (20) by reducing the second order ordinary differential equation system to the system of first order equations.

The inequality (43) defines a restriction on the allowable value of payload swaying. The condition (46) defines a restriction on the control voltage value and the allowable angular velocity of the crane boom slewing.

The absolute coordinates $x_{\mathrm{abs}}(t)$; $y_{\mathrm{abs}}(t)$; $z_{\mathrm{abs}}(t)$ of swaying payload M in the fixed inertial reference frame $\mathscr{E}$ may be computed as:

$$\begin{cases} x_{\mathrm{abs}}(t) = x_2^*(t) = (R + y_1(t))\cdot\cos(\varphi_{\mathrm{e}}(t)) + x_1(t)\cdot\sin(\varphi_{\mathrm{e}}(t)); \\ y_{\mathrm{abs}}(t) = y_2^*(t) = (R + y_1(t))\cdot\sin(\varphi_{\mathrm{e}}(t)) - x_1(t)\cdot\cos(\varphi_{\mathrm{e}}(t)); \\ z_{\mathrm{abs}}(t) = z_2^*(t) = z_1(t). \end{cases} \tag{50}$$

Differential Eqs. (35)–(42), which are proposed in the present work, describe the behavior of the mechanical system "crane boom–payload". These differential equations are written in implicit form, i.e., they have not been resolved with respect to the first derivatives in contrast to the optimal control problems addressed by Sakawa [9] and Terashima [10].

JModelica's [4] extension Optimica was used in the present work for a numerical solution of the open-loop optimal control problem. The direct method for numerical solution of the open-loop optimal control problem in Optimica is based on the conversion of the open-loop optimal control problem to the problem of nonlinear programming [1]. This approach allowed us to easily take into account the limitations on the phase and control variables in contrast to the indirect methods, which are grounded on the use of Pontryagin's maximum principle and addressed by Sakawa [9] and Terashima [10]. Sakawa et al. have addressed the Constraining Hyperplane Technique and penalty function approach in order to take into account the limitations on the phase and control variables [9].

The JModelica and Optimica codes are listed in Appendices 1, 2. The first lines of the *.mop Optimica-file in Appendix 1 determine the minimized function. In the present problem we optimize the time of payload transportation from the initial to the final position of the crane boom. Then we define the phase variables ($x_1(t)$, … , $x_8(t)$), which determine the system position at every time t and depend on the control input variable $u(t)$. Further we determine constant parameters of the model which include payload mass, crane boom length, cable length, and the values of limitations on the control and phase variables. The differential equations, which determine dynamic

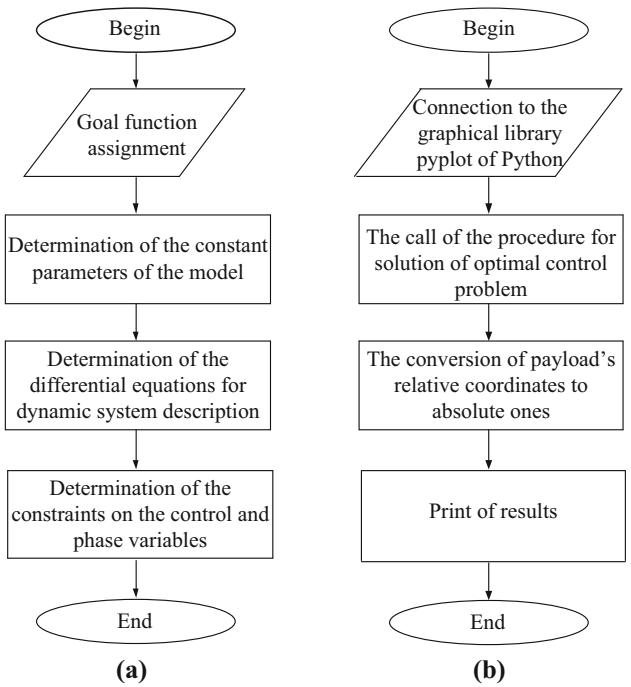

Fig. 2 The block diagrams of computational data flow within freeware codes Optimica (**a**) and JModelica.org (**b**)

system behavior, are written in the equation block of *.mop file (Appendix 1). In the constraint block we define limitations on the control and phase variables. The first eight limitations determine the final position of payload. The limitation $(x_1(t))^2 + (x_3(t))^2 + (x_5(t))^2 \leq \varepsilon$ determines the maximum value of payload swaying during crane boom rotation at the required angular displacement. This limitation means that during the motion the swaying of the payload must not be too large in order to keep the payload safe. The limitation on the control input variable $u(t)$, which is the voltage supplied to the electrical drive, is determined by hardware specifications. The last limitation on the value of crane boom angular velocity is also determined by electrical drive specifications.

The structure of Optimica's *.mop file in Appendix 1 is shown in Fig. 2a and the structure of JModelica's *.py file in Appendix 2 is shown in Fig. 2b.

2.3 Results of numerical solution of time-optimal control problem

Computational plots in Figs. 3, 4, 5, 7, 8 have been derived for the following numerical values of system parameters, listed in Appendix 1: $m = 0.1$ (kg); $l = 0.825$ (m); $R = 0.492$ (m); $g = 9.81$ (m/s^2); $u_{\max} = 10$ (V); $\omega_{\max} = 0.15$ (rad/s); $T_\varphi = 0.015$ (s); $K_\varphi = 0.315$ (1/(sV)).

Computational plots in Figs. 3 and 5a, b show that all six phase variables ($x_1(t)$, …, $x_6(t)$) show oscillation graphics of their change with time t. The oscillating nature of these plots is assumed to be dynamic effects resulting from action of d'Alembert inertial forces $\mathbf{\Phi}_{\mathbf{e}}^{\boldsymbol{\tau}}$ (6), $\mathbf{\Phi}_{\mathbf{e}}^{\mathbf{n}}$ (7) and Coriolis inertia force $\mathbf{\Phi}_{\mathbf{cor}}$ (8).

The computational plot in Fig. 4b shows that crane boom BD slewing angle $\varphi_e(t)$ changes with time t according to an almost linear law. This results in the fact

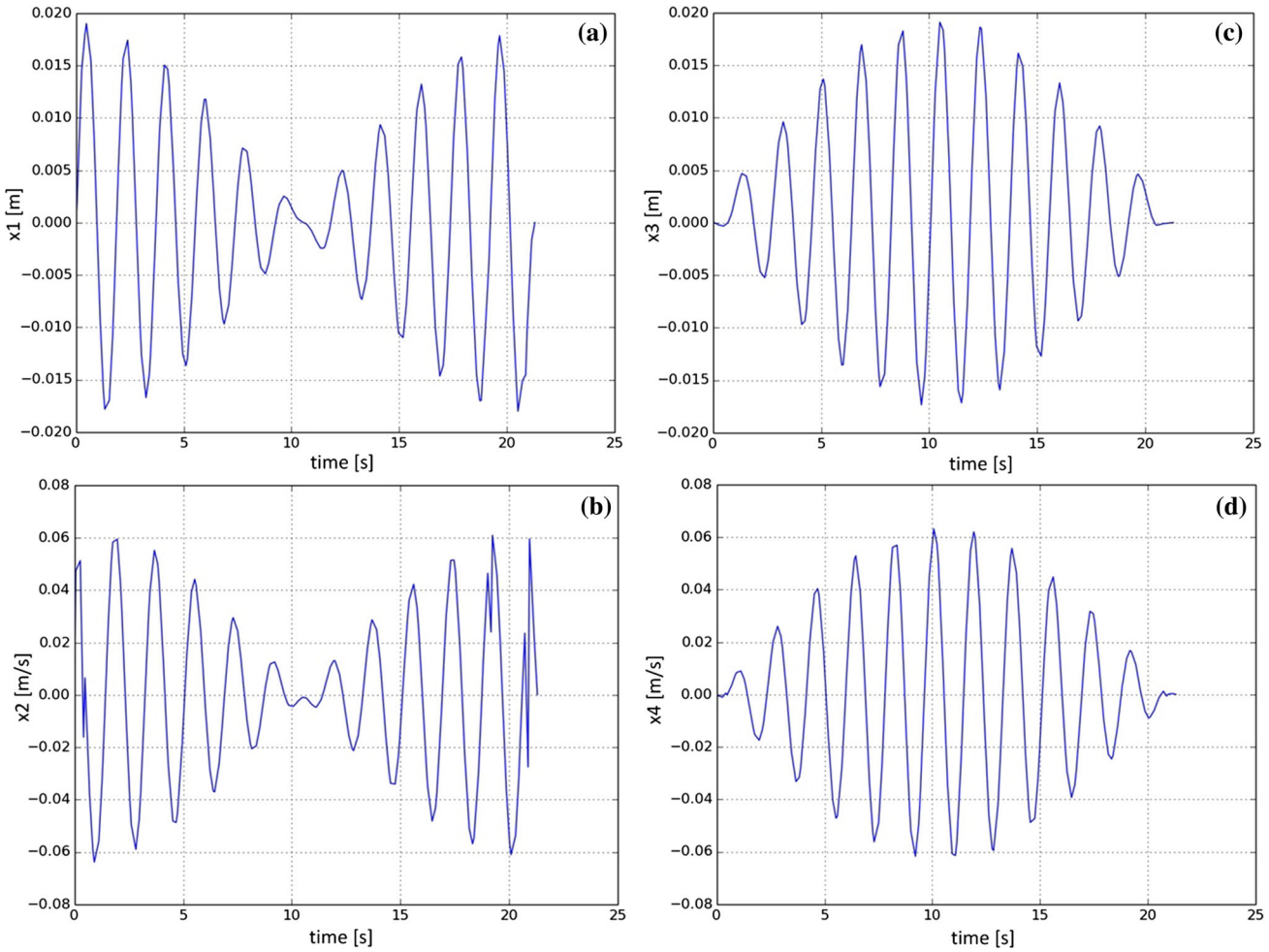

Fig. 3 The numerical plots for payload M computational relative coordinates $x_1 = x_1(t)$ (m) **a** and $y_1 = y_1(t)$ (m) **c** and relative velocity components $V_{x1} = \mathrm{d}(x_1(t))/\mathrm{d}t$ (m/s) **b** and $V_{y1} = \mathrm{d}(y_1(t))/\mathrm{d}t$ (m/s) **d** with respect to time t (s) in the non-inertial reference frame $\mathscr{B}$, derived with JModelica.org and Optimica for the codes in Appendices 1, 2

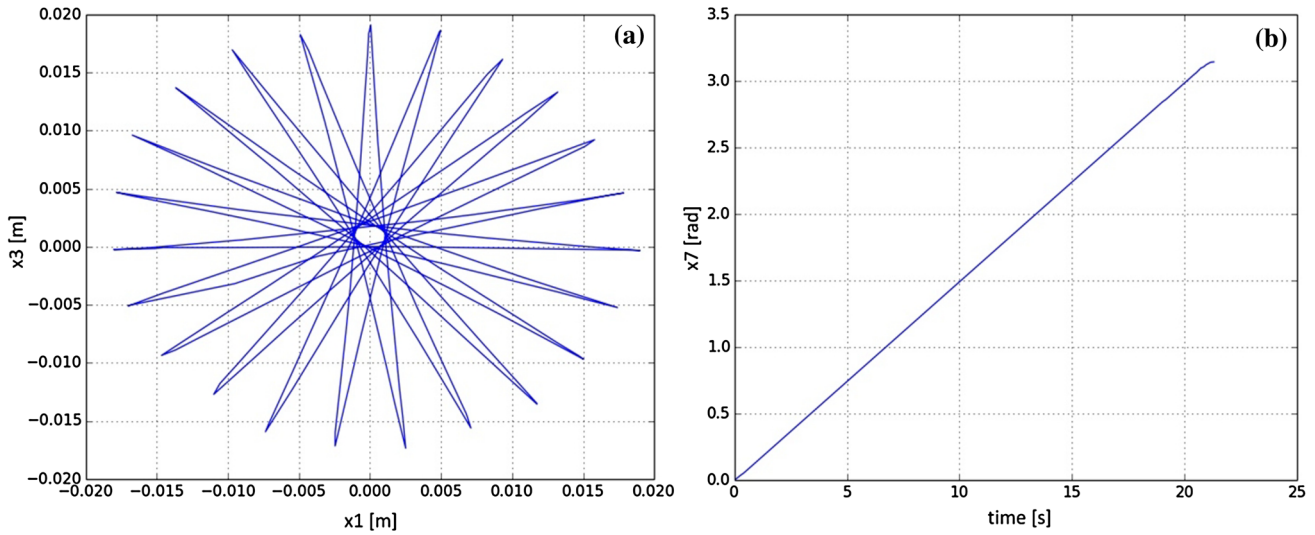

Fig. 4 The numerical plots for payload M computational relative trajectory $y_1 = y_1(x_1)$ (m) in the non-inertial reference frame $\mathscr{B}$ **a** and crane boom BD (Fig. 1) slewing angle $\varphi_e = \varphi_e\,(t)$ (rad) **b** derived with JModelica.org and Optimica for the codes in Appendices 1, 2

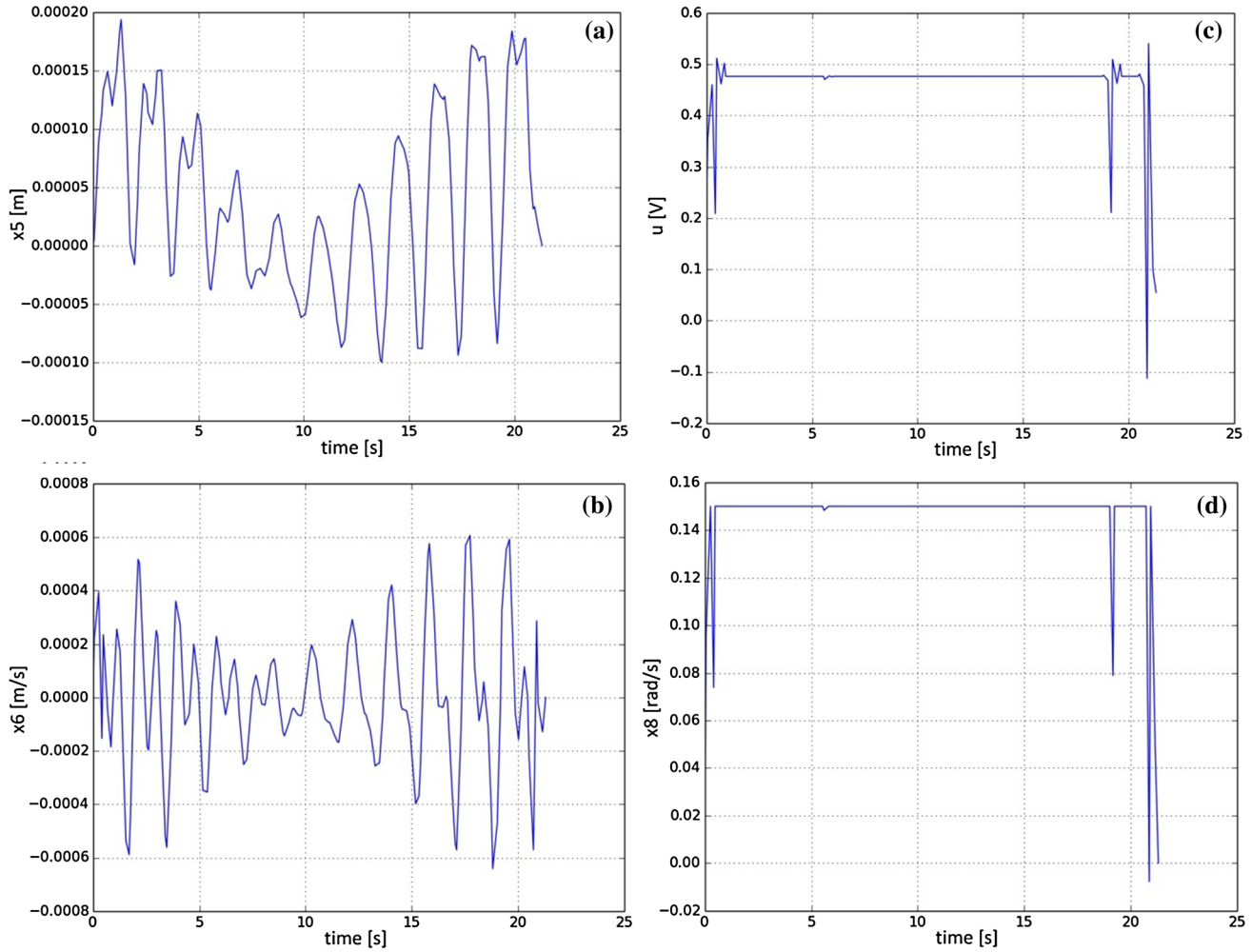

Fig. 5 The numerical plots for payload M computational relative coordinate $z_1 = z_1(t)$ (m) **a** and relative velocity component $V_{z1} = \mathrm{d}(z_1(t))/\mathrm{d}t$ (m/s) **b** in the non-inertial reference frame $\mathscr{B}$, and time curves (t, [s]) for control variable $u = u(t)$ (V) **c** and angular velocity $\omega_e = \mathrm{d}(\varphi_e\,(t))/\mathrm{d}t$ (rad/s) **d** of crane boom BD (Fig. 1) transport slewing, derived with JModelica.org and Optimica for the codes in Appendices 1, 2

that crane boom BD slewing angular velocity ω_e (t) in Fig. 5d remains almost constant (ω_e (t) $\approx$ const). However, Fig. 5c, d have two peak values at the beginning and at the end of crane boom BD slewing motion. The source of these peaks in Fig. 5c, d is associated with additional crane boom accelerations at the starting and stopping of rotary AC-servo motor.

3 Discussion, comparison and experimental verification of derived results

3.1 Physical simulation approach to experiment

For experimental verification of computational results an experimental setup was designed and installed (Fig. 6). The experimental measurement system in Fig. 6 uses a subscale physical simulation approach.

The upper digital camera has the large exposure time and camera's objective lens was opened up for 90 s (Figs. 7, 8). This time was enough to write the absolute trajectory of payload M swaying in an obscured room with the experimental setup (Fig. 6). A laser pointer was fixed on the boom tip B. The point O_1 was the horizontal point-projection of laser beam BO_1. Laser point O_1 drew the standard circular trajectory (— — — —) in Figs. 6, 7 and 8. The physical model of payload M was a light-emitting diode with diameter 2 mm and with the battery voltage 3 V. The luminous trace of payload M in the inertial reference frame $\mathscr{E}$ is shown as solid line

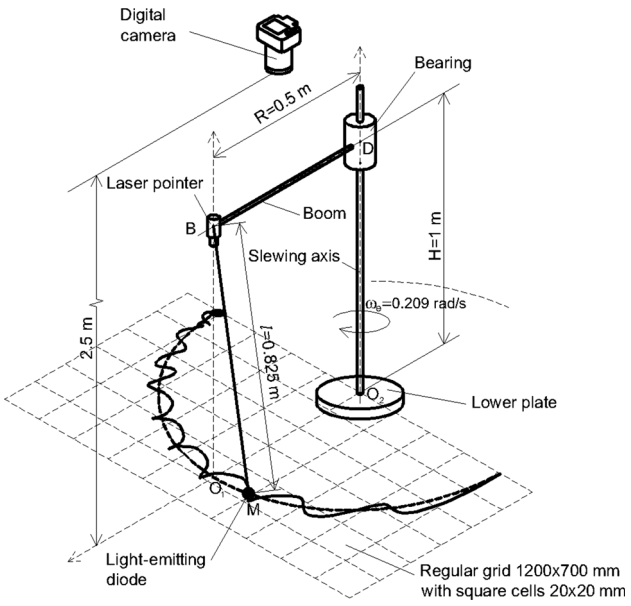

Fig. 6 The scheme of the experimental setup, designed for identification and measurement of absolute payload M trajectory in the inertial reference frame $\mathscr{E}$

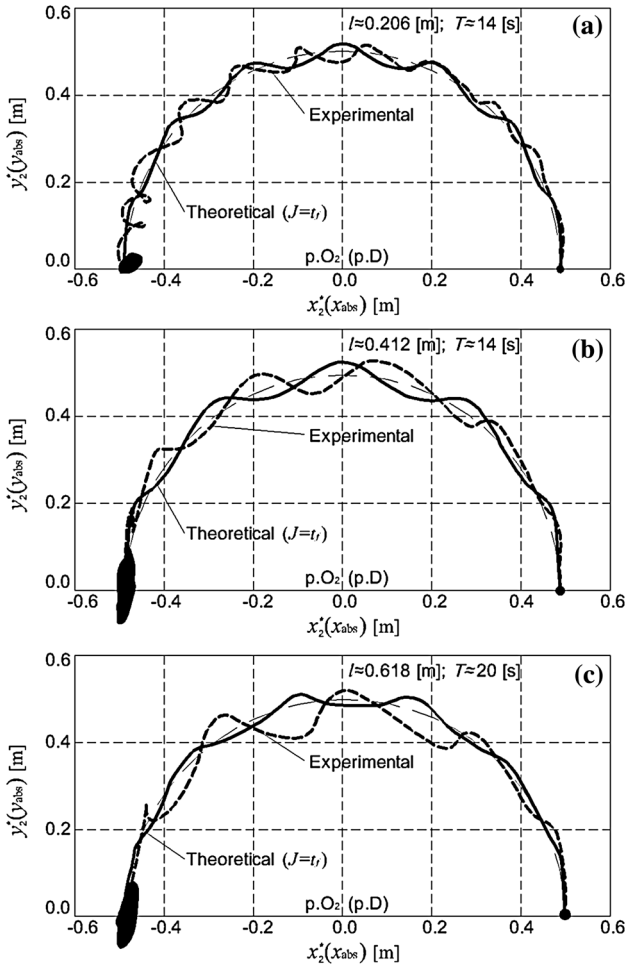

Fig. 7 The comparison of time-optimal control ($J = t_f$)-derived theoretical (*filled dashed line*) and experimental (*space filled dashed line*) absolute trajectories $y_{abs} = y_{abs}$ (x_{abs}) of payload M in the inertial reference frame $\mathscr{E}$ for the fixed cable lengths $l = 0.206$ (m) (**a**), $l = 0.412$ (m) (**b**), and $l = 0.618$ (m) (**c**)

(——————) in Fig. 6 and as a bold dashed line (— — — —) in Figs. 7 and 8.

The experimental swaying results in Fig. 6 (——————) and (— — — —) in Figs. 7 and 8 clearly show us that the forms of these experimental curves are shaped by Coriolis effects. So it is principally important to properly take into account Coriolis effects in mathematical models of payload M swaying during guided crane boom BD slewing.

3.2 Discussion and comparison of derived results with experiment

Small levels of payload swaying could be reached for the small angular velocities of crane boom slewing. So it is possible to show good agreement between theoretical and

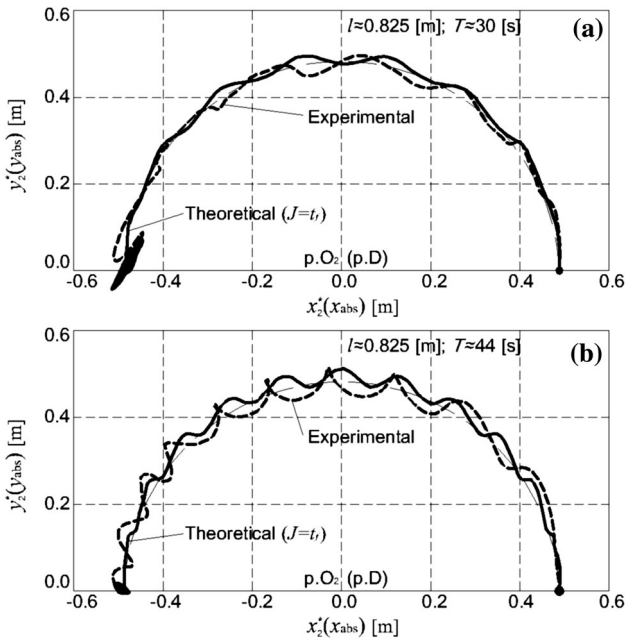

Fig. 8 The comparison of time-optimal control ($J = t_f$)-derived theoretical (*filled dashed line*) and experimental (*space filled dashed line*) absolute trajectories $y_{abs} = y_{abs}\,(x_{abs})$ of payload M in the inertial reference frame $\mathscr{E}$ with the fixed cable length $l = 0.825$ (m) for $T = 30$ (s) (**a**) and $T = 44$ (s) (**b**)

computational results by the assignment of a small value of payload swaying into the mathematical model.

The comparison of theoretical numerical solution of time-optimal control problem (34)–(46) (▬▬▬▬▬, $y_{abs} = y_{abs}\,(x_{abs})$ or $y_2^* = y_2^*\,(x_2^*)$) and experimental (▬ ▬ ▬ ▬, $y_{abs} = y_{abs}\,(x_{abs})$ or $y_2^* = y_2^*\,(x_2^*)$) results is shown in Figs. 7 and 8. In order to estimate the relative disagreement of the derived time-optimal control-solution based computational (▬▬▬▬▬) and experimental (▬ ▬ ▬ ▬) payload M absolute trajectories in the inertial reference frame $\mathscr{E}$ we have computed the amplitude discrepancy δ in the polar coordinate system by the following formula:

$$\delta = \left\langle \frac{1}{2}\left(\left(\frac{\left|r_{comp} - r_{exper}\right|}{r_{comp}}\right) + \left(\frac{\left|r_{comp} - r_{exper}\right|}{r_{exper}}\right)\right)\right\rangle, \tag{51}$$

where r_{comp} and r_{exper} are the magnitudes of the radius-vectors, connecting point O_2 and theoretical ($J = t_f$)-based computational (▬▬▬▬▬) and experimental (▬ ▬ ▬ ▬) curves, and computed for the same fixed polar angle φ_e, and r_{circle} is the radius of standard circular trajectory (— — — —) of p. B (p. A $_{st}$) in Figs. 1 and 6.

The amplitude discrepancies δ have the following values: $\delta = 3.86$ % and $\delta_{max} = 8.47$ % for $l = 0.206$ (m) in Fig. 7a; $\delta = 5.01$ % and $\delta_{max} = 11.93$ % for $l = 0.412$ (m) in Fig. 7b; $\delta = 5.67$ % and $\delta_{max} = 18.88$ % for $l = 0.618$ (m) in Fig. 7c; $\delta = 2.33$ % and $\delta_{max} = 6.79$ % for $l = 0.825$ (m) and $T = 30$ (s) in Fig. 8a and $\delta = 4.36$ % and $\delta_{max} = 11.94$ % for $l = 0.825$ (m) and $T = 44$ (s) in Fig. 8b.

For further estimation of the relative disagreement of derived time-optimal control-solution based ($J = t_f$) computational (▬▬▬▬▬) absolute trajectory of payload M, experimental (▬ ▬ ▬ ▬) payload M absolute trajectory and standard circular trajectory (— — — —) of p. B (p. A $_{st}$) (Figs. 1, 6) in the inertial reference frame $\mathscr{E}$ we have computed the confidence intervals in Figs. 7 and 8 for the dimensionless radii parameters r_{circle}/r_{exper}; r_{circle}/r_{comp}; r_{comp}/r_{exper}, and confidence probabilities 0.95 and 0.99. The Student's t test results yield the following confidence intervals, shown in Table 1. Both the relative discrepancy δ and the confidence intervals in Table 1 show the satisfactory agreement between the absolute payload trajectories (Figs. 7, 8) in the inertial reference frame $\mathscr{E}$, that have been computed with theoretical numerical solution of time-optimal control problem (34)–(46) (▬▬▬▬▬, $y_{abs} = y_{abs}\,(x_{abs})$ or $y_2^* = y_2^*\,(x_2^*)$), and measured experimentally (▬ ▬ ▬ ▬, $y_{abs} = y_{abs}\,(x_{abs})$ or $y_2^* = y_2^*\,(x_2^*)$) as shown in Figs. 7 and 8.

3.3 Discussion and comparison of derived results with known published results

The computational results in Figs. 7 and 8, derived with a numerical solution of the time-optimal control problem (34)–(46) were also compared with known published Sakawa's [9] result. The graphical result of the comparison is shown in Fig. 9.

Comparative analysis of Fig. 9 shows the essential discrepancies between our derived result (▬▬▬▬▬) and Sakawa's [9] published result (▬ ▬ ▬ ▬). The amplitude discrepancies δ, which were computed with formula (51), have the following values: $\delta = 5$ % and $\delta_{max} = 12.37$ % for two curves in Fig. 9. The Student's t test results yield the following confidence intervals for the amplitude discrepancies δ: for confidence probability 0.90 we have the confidence interval $3.29\ \% \le \delta \le 6.75\ \%$; for confidence probability 0.95 we have the confidence interval $2.96\ \% \le \delta \le 7.08\ \%$; and for confidence probability 0.95 we have the confidence interval $2.31\ \% \le \delta \le 7.73\ \%$.

The differences between these curves result from taking into account the Coriolis effects in our ($J = t_f$) theoretical solution. Coriolis effects cause additional changes of shape in our absolute trajectory (▬▬▬▬▬) in the inertial reference frame $\mathscr{E}$. Our experimental results in Figs. 7 and

Table 1 The confidence intervals for comparison of ($J = t_f$)-derived theoretical and experimental absolute trajectories $y_{abs} = y_{abs}$ (x_{abs}) of payload M in the inertial reference frame $\mathscr{E}$

	Confidence probability 0.95			Confidence probability 0.99		
	$\left(\frac{r_{cir}}{r_{emp}}\right)_{0.95}$	$\left(\frac{r_{circ}}{r_{emp}}\right)_{0.95}$	$\left(\frac{r_{comp}}{r_{emp}}\right)_{0.95}$	$\left(\frac{r_{cir}}{r_{emp}}\right)_{0.99}$	$\left(\frac{r_{circ}}{r_{comp}}\right)_{0.99}$	$\left(\frac{r_{comp}}{r_{emp}}\right)_{0.99}$
$l = 0.206$ (m) and $T = 14$ (s) in Fig. 6a	$0.9882655 \leq (r_{circle}/r_{exper})_{0.95} \leq 0.9890754$	$0.9944104 \leq (r_{circle}/r_{comp})_{0.95} \leq 0.9947147$	$0.9940598 \leq (r_{comp}/r_{exper})_{0.95} \leq 0.9952771$	$0.9881302 \leq (r_{circle}/r_{exper})_{0.99} \leq 0.9892107$	$0.9943596 \leq (r_{circle}/r_{comp})_{0.99} \leq 0.9947655$	$0.9938565 \leq (r_{comp}/r_{exper})_{0.99} \leq 0.9954805$
$l = 0.412$ (m) and $T = 14$ (s) in Fig. 6b	$0.9813904 \leq (r_{circle}/r_{exper})_{0.95} \leq 0.9823100$	$0.9906246 \leq (r_{circle}/r_{comp})_{0.95} \leq 0.9911901$	$0.9913016 \leq (r_{comp}/r_{exper})_{0.95} \leq 0.9933036$	$0.9812374 \leq (r_{circle}/r_{exper})_{0.99} \leq 0.9824630$	$0.9905306 \leq (r_{circle}/r_{comp})_{0.99} \leq 0.9912842$	$0.9909685 \leq (r_{comp}/r_{exper})_{0.99} \leq 0.9936367$
$l = 0.618$ (m) and $T = 20$ (s) in Fig. 6c	$1.0257253 \leq (r_{circle}/r_{exper})_{0.95} \leq 1.0280459$	$0.9867881 \leq (r_{circle}/r_{comp})_{0.95} \leq 0.9869449$	$1.0395866 \leq (r_{comp}/r_{exper})_{0.95} \leq 1.0422741$	$1.0253377 \leq (r_{circle}/r_{exper})_{0.99} \leq 1.0284334$	$0.9867620 \leq (r_{circle}/r_{comp})_{0.99} \leq 0.9869711$	$1.0391378 \leq (r_{comp}/r_{exper})_{0.99} \leq 1.0427229$
$l = 0.825$ (m) and $T = 30$ (s) in Fig. 7a	$1.0048594 \leq (r_{circle}/r_{exper})_{0.95} \leq 1.0053250$	$0.9921185 \leq (r_{circle}/r_{comp})_{0.95} \leq 0.9922326$	$1.0128811 \leq (r_{comp}/r_{exper})_{0.95} \leq 1.0134405$	$1.0047799 \leq (r_{circle}/r_{exper})_{0.99} \leq 1.0054046$	$0.9920989 \leq (r_{circle}/r_{comp})_{0.99} \leq 0.9922521$	$1.0127855 \leq (r_{comp}/r_{exper})_{0.99} \leq 1.0135360$
$l = 0.825$ (m) and $T = 44$ (s) in Fig. 7b	$1.0071221 \leq (r_{circle}/r_{exper})_{0.95} \leq 1.0088435$	$0.9892011 \leq (r_{circle}/r_{comp})_{0.95} \leq 0.9894176$	$1.0181160 \leq (r_{comp}/r_{exper})_{0.95} \leq 1.0196874$	$1.0068338 \leq (r_{circle}/r_{exper})_{0.99} \leq 1.0091318$	$0.9891649 \leq (r_{circle}/r_{comp})_{0.99} \leq 0.9894539$	$1.0178529 \leq (r_{comp}/r_{exper})_{0.99} \leq 1.0199505$

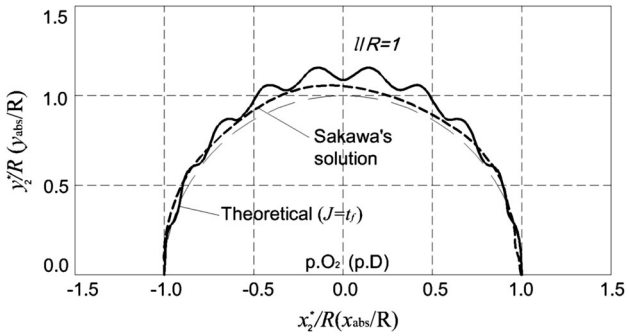

Fig. 9 Graphical comparison of computational absolute trajectories of payload M in the inertial reference frame $\mathscr{E}$, where (*filled dashed line*) is ($J = t_f$)-derived result (26)–(63) and (*space filled dashed line*) is Sakawa's [9] published solution

8 additionally indicate that it is necessary to take Coriolis effects into account for a correct simulation of swaying payload dynamics during crane boom BD slewing.

4 Discussion

I. The present work is focused on a study of payload swaying during guided crane boom slewing, taking into account the Coriolis effects. The formulation of the dynamic problem was made with the use of Blajer's [2] mathematical formalism. Introduction of Blajer's approach provided us with a useful and physically clear mathematical technique for derivation of motion equations for payload swaying and with a simple way for determination of constraint reaction $\lambda(t) = N(t)$. Blajer's projection's method was used in this work for derivation of dynamic Eqs. (19)–(22), (25). Application of Blajer's projection's technique was based on the projection of Blajer's governing Eq. (17) for the motion of the constrained mechanical system "crane boom BD–payload M" in orthogonal and tangential directions to the surface of the geometric constraint (18). It is possible to obtain an expression of the constraint reaction $\lambda(t) = N(t)$ with projection of the dynamic governing Eq. (17) in the orthogonal direction to the surface of the geometric constraint (18). It is possible to derive the motion equations, which are free from constraint reaction forces $\lambda(t) = N(t)$, with projection of the dynamic governing Eq. (17) in the tangential direction to the surface of the geometric constraint (18). Blajer et al. have applied their approach for building a control of boom cranes, which has to provide the prescribed motion for the payload during crane boom transportation. In contrast to Blajer's approach, our dynamic Eqs. (9)–(11) were written in the non-inertial reference frame $\mathscr{B}$ in order to take into account the Coriolis inertia force. Introduction of Blajer's mathematical formalism in the present article demonstrates the success and sustainability of Blajer's approach to the formulation of the dynamic problem of

payload swaying during guided crane boom slewing, taking into account the Coriolis effects.

II. For small values of payload swaying restriction ε the numerical solution of the time-optimal control problem results in the fact that the optimum motion for the crane boom is the slewing motion with constant angular velocity. For larger values of payload swaying ε the angular velocity of the crane boom is not constant and changes with time according to a nonlinear law. Coriolis effects on the relative (Fig. 4a) and absolute (Figs. 6, 7, 8) trajectories of guided payload M are especially essential for small slewing velocities in controlled crane boom rotation. Small values of crane boom BD-guided angular rotation have large importance for all practical applications in the field of guidance and accurate positioning with lifting-and-handling machinery. Indeed, large slewing velocities of a crane boom are outside the aims and scopes of boom crane-assisted practical problems. The absolute computational trajectories in Figs. 6, 7, 8 are the numerical JModelica.org-derived solutions of the time-optimal control problem.

III. The solution of the open-loop optimal control problem in Figs. 3, 4, 5, 7, 8 shows that under the given problem conditions the crane boom BD rotates nearly uniformly in Fig. 4b (i.e., angular velocity of crane boom BD transport slewing is almost constant in Fig. 5c, d). In this case the trajectory of the relative payload M swaying with respect to the uniformly rotating crane boom BD is the so-called Foucault pendulum-like curve (Fig. 4a). So the present article extends the ideas about adaptability of Foucault pendulum-like systems for the problems of open-loop optimal control for swaying of the spherical pendulum with rotating pivot center. For the solution of the time-optimal control problem the constancy of angular crane boom slewing velocity takes place for small values of the restriction ε on payload swaying in formulae (43) and small values of the crane boom slewing velocity $\omega_e = d(\varphi_e)/dt$ (limitation at $x_8(t)$) in formulae (46). Increase in the limitation ω_{max} on the value of $x_8(t)$ results in large swaying of the payload, resulting from large accelerations in the beginning and at the end of payload motion. The relative trajectory of payload M swaying with respect to non-uniformly rotating crane boom BD, associated with non-inertial reference frame $\mathscr{B}$ in Fig. 1, has been numerically derived in the present work through the JModelica.org and Optimica-based solution of $J = t_f$ time-optimal control problem (34)–(46) and Appendices 1, 2 and is shown in Fig. 4a. The relative trajectories of a Foucault pendulum swaying with respect to a uniformly rotating Earth-associated non-inertial reference frame $\mathscr{E}$ have been shown by Condurache and Martinusi (2008) in Eq. (4.33) and Fig. 16, p. 755 of [3]. Comparison of computational relative trajectories in the present work and in Ref. [3] describes the similarity between these relative trajectories. So it is possible to conclude that the relative swaying motion of a spherical pendulum with guided non-uniform rotation of the pivot center in Figs. 1, 4a and 6 of the present study can be described as Foucault pendulum-like motion.

5 Conclusions

I. The present work has developed and studied a dynamic model of payload motion during non-uniform crane boom slewing with an emphasis on Coriolis effects. The derivation of the governing dynamic equations was made with the use of Blajer's mathematical formalism and Blajer's projection method. Time-optimal control problem was formulated with the use of derived governing equations for the motion of the system "crane boom–payload". By solving the time-optimal control problem we find the control input function $u(t)$, which allows the transport of the payload from the initial to the final position with minimum transportation time.

II. The numerical solution of the time-optimal control problem has been derived with an introduction of Optimica and JModelica.org freeware. The graphical results of numerical simulation of the absolute trajectories of payload swaying were compared with experimental results. The comparison of theoretical and experimental results showed a satisfactory agreement between numerically derived and empirical data. The results of numerical analysis have extended our ideas about dynamics of the guided Foucault pendulum-like systems.

III. Further analysis of pendulum swaying problems during controlled crane boom slewing is promising through the building of closed-loop control, the introduction of additional degrees of freedom into the model of guided payload motion (variable cable length, an arbitrary rectilinear motion of pendulum pivot center B along crane boom BD, etc.) and by taking into account random wind load, as well as additional forced vibrations, generated from the oscillating foundation (point O_2 in Figs. 1 and 6) in offshore- and ocean-engineering related problems.

Acknowledgments Authors thank "anonymous" referees for their valuable notes and suggestions.

Compliance with ethical standards

Conflict of interest The authors Alexander A. Kostikov, Alexander V. Perig, Denys Yu. Mikhieienko, and Ruslan R. Lozun declare that there is no conflict of interests regarding the publication of this paper.

Disclosure The submission of the authors' paper implies that it has not been previously published, that it is not under consideration for publication elsewhere, and that it will not be published elsewhere in the same form without the written permission of the editors.

Appendix 1: Listing of the *.mop Optimica's file

```
optimization RcraneOne(objective = finalTime,
startTime = 0,finalTime(free=true,min = 1,max = 45,
initialGuess=6))
Real x1(start=x1_0,fixed=true);
Real x2(start=x2_0,fixed=true);
Real x3(start=x3_0,fixed=true);
Real x4(start=x4_0,fixed=true);
Real x5(start=x5_0,fixed=true);
Real x6(start=x6_0,fixed=true);
Real x7(start=x7_0,fixed=true);
Real x8(start=x8_0,fixed=true);


input Real u;


 parameter Real x1_0=0;
 parameter Real x2_0=0;
 parameter Real x3_0=0;
 parameter Real x4_0=0;
 parameter Real x5_0=0;
 parameter Real x6_0=0;
 parameter Real x7_0=0;
 parameter Real x8_0=0;

 parameter Real m=0.1;
 parameter Real R=0.492;
 parameter Real g=9.81;
 parameter Real l=0.825;
 parameter Real n_0=m*g;
 parameter Real u_max=10;
 parameter Real v_max=0.15;

 parameter Real TS=0.015;
 parameter Real KS=0.315;

 parameter Real K1=-1/TS;
 parameter Real K2=KS/TS;

 parameter Real x1_N=0;
 parameter Real x2_N=0;
 parameter Real x3_N=0;
 parameter Real x4_N=0;
 parameter Real x5_N=0;
 parameter Real x6_N=0;
 parameter Real x7_N=3.1415926;
```

```
parameter Real x8_N=0;


equation

der(x1)=x2;
der(x2)=x8^2*x1+(K1*x8+K2*u)*(R+x3)+2*x8*x4-
((m*l*((x1*der(x2)+x2^2+x3*der(x4)+x3^2)*(l^2-x1^2-x3^2)+(x1*x2+x3*x4)^2)/(l^2-x1^2-
x3^2)+m*g*l/sqrt(l^2-x1^2-x3^2))/m)*(x1/l);
der(x3)=x4;
der(x4)=x8^2*(R+x3)-(K1*x8+K2*u)*x1-2*x8*x2-
((m*l*((x1*der(x2)+x2^2+x3*der(x4)+x3^2)*(l^2-x1^2-x3^2)+(x1*x2+x3*x4)^2)/(l^2-x1^2-
x3^2)+m*g*l/sqrt(l^2-x1^2-x3^2))/m)*(x3/l);
der(x5)=x6;
der(x6)=-g+((m*l*((x1*der(x2)+x2^2+x3*der(x4)+x3^2)*(l^2-x1^2-
x3^2)+(x1*x2+x3*x4)^2)/(l^2-x1^2-x3^2)+m*g*l/sqrt(l^2-x1^2-x3^2))/m)*(l-x5)/l;
der(x7)=x8;
der(x8)=K1*x8+K2*u;


constraint
x1(finalTime)=0;
x2(finalTime)=0;
x3(finalTime)=0;
x4(finalTime)=0;
x5(finalTime)=0;
x6(finalTime)=0;
x7(finalTime)=3.1415;
x8(finalTime)=0;
x1^2+x3^2+x5^2<=0.01;
-u_max<=u;
u<=u_max;
-v_max<=x8;
x8<=v_max;

end RcraneOne;
```

Appendix 2: Listing of the *.py JModelica's file

```
from pyjmi import transfer_optimization_problem
import matplotlib.pyplot as plt
import math
import numpy as N
def f(t):
    return N.sqrt(0.492*0.492-t*t)
op = transfer_optimization_problem('RcraneOne',
'RCraneOne9.mop')
res = op.optimize()
t = res['time']
x1 = res['x1']
x2 = res['x2']
x3 = res['x3']
x4 = res['x4']
x5 = res['x5']
x6 = res['x6']
x7 = res['x7']
x8 = res['x8']
u = res['u']
r1=0.492
p1=(r1+x3)*N.cos(x7)+x1*N.sin(x7)
p2=(r1+x3)*N.sin(x7)-x1*N.cos(x7)
y=f(p1)
with open("out.txt","w") as out:
  for i in range(len(p1)):
   print(str(p1[i])+' '+str(p2[i]))

#f = open("out.txt",'w')
#f.close
plt.figure(1)
plt.clf()

plt.subplot(421)
plt.plot(p1,p2)
plt.grid()
plt.ylabel('p1')
plt.xlabel('p2')

plt.subplot(422)
plt.plot(t,x1)
plt.grid()
plt.ylabel('x1')
plt.xlabel('time')

plt.subplot(423)
plt.plot(t,x3)
plt.grid()
plt.ylabel('x3')
plt.xlabel('time')

plt.subplot(424)
plt.plot(t,x5)
plt.grid()
plt.ylabel('x5')
plt.xlabel('time')

plt.subplot(425)
plt.plot(t,x7)
plt.grid()
plt.ylabel('x7')
plt.xlabel('time')

plt.subplot(426)
plt.plot(t,u)
plt.grid()
plt.ylabel('u')
plt.xlabel('time')

plt.subplot(427)
plt.plot(t,x8)
plt.grid()
plt.ylabel('x8')
plt.xlabel('time')
```

```
plt.subplot(428)
plt.plot(x1,x3)
plt.grid()
plt.ylabel('x1')
plt.xlabel('x3')

plt.figure(3)
plt.clf()

plt.subplot(111)
plt.plot(p1,p2,linewidth=2.0)
plt.plot(p1,y,'g--')
plt.xlim(-0.6,0.6)
plt.ylim(0.0,0.948)
plt.grid()
plt.ylabel('p1')
plt.xlabel('p2')

plt.figure(2)
plt.clf()
plt.subplot(111)

plt.plot(p1,p2,linewidth=2.0)
plt.xlim(-0.6,0.6)
plt.ylim(0.0,0.948)
plt.grid()
plt.ylabel('p1')
plt.xlabel('p2')

plt.figure(4)
plt.clf()

plt.subplot(111)
plt.plot(x1,x3)

plt.grid()
plt.ylabel('x3')
plt.xlabel('x1')
plt.show()
```

References

1. Benson DA, Huntington GT, Thorvaldsen TP, Rao AV (2006) Direct trajectory optimization and costate estimation via an orthogonal collocation method. J Guid Control Dyn 29(6):1435–1440. doi:10.2514/1.20478
2. Blajer W, Kołodziejczyk K (2006) Dynamics and control of rotary cranes executing a load prescribed motion. J Theor Appl Mech 44(4):929–948
3. Condurache D, Martinusi V (2008) Foucault pendulum-like problems: a tensorial approach. Int J Nonlinear Mech 43:743–760. doi:10.1016/j.ijnonlinmec.2008.03.009
4. Modelon AB (2015) JModelica.org user guide: Version 1.17. 175 pp. Available from internet http://www.jmodelica.org/api-docs/usersguide/JModelicaUsersGuide-1.17.0.pdf. Accessed 28 May 2016
5. Palis F, Palis S (2008) High performance tracking control of automated slewing cranes. In: Balaguer C, Abderrahim M (eds) Robotics and automation in construction, InTech, pp 187–198. doi: 10.5772/5851
6. Perig AV, Stadnik AN, Deriglazov AI (2014) Spherical pendulum small oscillations for slewing crane motion. ScientificWorldJournal, p 10 (Article ID 451804). doi: 10.1155/2014/451804
7. Perig AV, Stadnik AN, Deriglazov AI, Podlesny SV (2014) 3 DOF spherical pendulum oscillations with a uniform slewing pivot center and a small angle assumption. Shock Vib, p 32 (Article ID 203709). doi: 10.1155/2014/203709
8. Pontryagin LS, Boltyanskii VG, Gamkrelidze RV, Mishchenko EF (1962) The mathematical theory of optimal processes. Wiley, New York, p 360
9. Sakawa Y, Shindo Y, Hashimoto Y (1981) Optimal control of a rotary crane. J Optim Theory Appl 35(4):535–557. doi:10.1007/BF00934931
10. Terashima K, Shen Y, Yano K (2007) Modeling and optimal control of a rotary crane using the straight transfer transformation method. Control Eng Pract 15(9):1179–1192. doi:10.1016/j.conengprac.2007.02.008